Dyes and Pigments 188 (2021) 109208

Contents lists available at ScienceDirect

Dyes and Pigments

journal homepage: http://www.elsevier.com/locate/dyepig

Adjusting the photophysical properties of AIE-active TADF emitters from through-bond to through-space charge transfer for high-performance solution-processed OLEDs

Fulong Ma [a], Hefang Ji [a], Dongdong Zhang [a], Ke Xue [a], Pan Zhang [a], Zhengjian Qi [a,*], Huaiyuan Zhu [b,**]

[a] School of Chemistry and Chemical Engineering, Southeast University, Nanjing, Jiangsu, 211189, PR China
[b] China Tobacco Jiangsu Industrial Co., Ltd., Nanjing, Jiangsu, 210019, PR China

ARTICLE INFO

Keywords:
Aggregation-induced emission
Thermally activated delayed fluorescence
Solution-processed
Through-space charge transfer
Organic light-emitting diodes

ABSTRACT

Intramolecular through-space charge transfer (TSCT) excited state has been exploited for developing thermally activated delayed fluorescence (TADF) emitters, while the adjustment of excited state dynamics by conformational engineering is still rare. Herein, we designed a series of AIE-active TADF emitters, bearing triphenylamine as donor and phenyl ketone as acceptor unit, and the evolution of charge transfer from through-bond to through-space is realized by controlling the relative position of the donor and acceptor units. Upon transforming the charge transfer categories from through-bond to through-space, the reverse intersystem crossing (RISC) rate is progressively improved by virtue of the narrower energy split between singlet and triplet states (ΔE_{ST}), meanwhile, the restricted intramolecular motion suppresses the non-radiative decay effectively, resulting in obviously improved luminescence efficiency. Appointing a bipolar blue TADF material as host to sensitize these emitters, solution-processed organic light-emitting diodes (OLEDs) based on TSCT emitter **1TCPM-Cz** achieve maximum current efficiency (CE) of 35.5 cd A^{-1} and external quantum efficiency (EQE) of 13.3%, respectively, which is higher than that of through-bond charge transfer (TBCT) analogues. The work demonstrates a convenient design strategy to achieve high-performance TSCT emitters by regulating the conformation of the donor and acceptor.

1. Introduction

Over the past few years, thermally activated delayed fluorescence (TADF) materials have received much attention as it not only employs metal-free frameworks but also upconverts full triplet excitons into emissive singlet excitons via reverse intersystem crossing (RISC) for reaching ultrahigh external quantum efficiencies (EQEs) [1–8]. Therefore, endowing TADF emitters with fast RISC rate stemmed from very small energy difference between the singlet and triplet excited states (ΔE_{ST}) is most momentous to fabricate high-performance OLEDs [9–11]. For the aim of achieving a very small ΔE_{ST}, the separation of highest occupied molecular orbital (HOMO) and the lowest unoccupied molecular orbital (LUMO) is requisite which could be adjusted by tuning types of donor and acceptor, geometries and steric hindrance to generate intramolecular charge transfer (ICT) emission [12–16]. Therefore, to realize highly efficient TADF emitters, the properties of ICT states should be adjusted elaborately by regulating the electron interaction manner between donor and acceptor moieties.

Many highly efficient TADF emitters based on ICT including through bond charge transfer (TBCT) and through space charge transfer (TSCT) have been developed and applied into fabricating high-performance OLEDs [17–20]. In TBCT emitters, the donor and acceptor moieties are usually linked directly through single bond [21–23]. Being different from TBCT, TSCT occurs between donor and acceptor via spatial interaction [24–26]. For the aim of obtaining very small ΔE_{ST}, highly twisted angle between donor and acceptor is requisite, which compels TBCT emitters adopting appropriate donor or/and acceptor and high steric hindrance, limiting the establishment of novel TADF emitters via directly linking donor and acceptor fragments. Compared with TBCT, TSCT emitters have emerged as an appealing TADF candidate owing to its intrinsic small ΔE_{ST} of TSCT nature [27–29]. In addition, for enhancing photoluminescence quantum yields (PLQYs), restriction of

* Corresponding author.
** Corresponding author.
E-mail addresses: qizhengjian@seu.edu.cn (Z. Qi), zhuhy@jszygs.com (H. Zhu).

https://doi.org/10.1016/j.dyepig.2021.109208
Received 15 December 2020; Received in revised form 28 January 2021; Accepted 28 January 2021
Available online 2 February 2021

intramolecular motion should also be taken into account. In TBCT emitters, the donor and acceptor units are assembled directly via single bond, demonstrating the vibrant molecular rotary motion existed which will induce emission loss. Conversely, the free rotation in TSCT emitters is anticipated be restricted effectively due to the intense intramolecular interaction between donor and acceptor [30–32]. Therefore, realizing the evolution of charge transfer categories of TADF emitters from through-bond to through-space by succinctly controlling the relative position of the donor and acceptor units is significant to realize fast RISC and fabricate high-performance OLEDs.

Herein we constructed a set of AIE-active TADF emitters, bearing electron-donating triphenylamine and electron-accepting phenyl ketone. By appending the triphenylamine on the C3, C2, and C1 position of carbazole bridge, respectively, the electron interaction manner between donor and acceptor could be adjusted from through-bond to through-space. Owing to the narrower ΔE_{ST} induced by valid separation of donor and acceptor, faster RISC rate was realized, and the non-radiative decay could be suppressed effectively resulted from the restricted intramolecular motion, resulting in improved luminescence efficiency. Furthermore, in comparison with TBCT emitters, the TSCT displayed enhanced AIE properties due to the strongly suppressed non-radiative decay resulted from both highly twisted structures and restricted intramolecular motion between donor and the acceptor moieties. Nominating a blue TADF material as bipolar host, solution-processed OLEDs based on TSCT emitter of **1TCPM-Cz** achieve maximum current efficiency (CE) of 35.5 cd A^{-1} and external quantum efficiency (EQE) of 13.3%, respectively, surpassing the TBCT analogues. These work provide a convenient approach to develop highly efficient TSCT-type TADF emitters by transforming the charge transfer from through bond through space via regulating the conformation of donor and acceptor.

2. Experimental and characterization

2.1. General information

All experimental materials and solvents were obtained from commercial approach without any further purification if not particularly mentioned. ^{1}H NMR and ^{13}C NMR spectra were performed on a Bruker Advance 600 MHz using DMSO-d_6 and $CDCl_3$ as solvents at room temperature. Molecular masses were measured on matrix-assisted laser desorptionionization time-of-flight mass spectrometry (MALDI-TOF-MS) employing a BRUKER DALTONICS instrument and a-cyanohydroxycinnamic acid was chosen as a matrix. Elemental analyses were carried out on VARIO EL III. UV–Vis absorption spectra were obtained on UV-2600 (Shimadzu Corporation) and photoluminescence emission spectra were measured from Fluoromax-4 (Horiba Jobin Yvon Inc) spectrophotometer. The solid and solution PL quantum efficiencies of the targeted product were measured using an integrating sphere under N_2 at room temperature. Thermogravimetric analysis (TGA) was performed with Netzsch simultaneous thermal analyzer (STA) system (STA409 PC) under a N_2 flow at a heating rate of 10 °C min^{-1}. Differential scanning calorimetry (DSC) curves were tested using a Netzsch instrument (TA, Netzsch). Cyclic voltametry (CV) was performed in CH_2Cl_2 solution (10^{-3} M) with tetrabutylammonium hexafluorophosphate (0.1 M) as supporting electrolyte and ferrocene as the internal standard at a scan rate of 100 mV s^{-1} on CHI750C voltammetric analyzer. A platinum plate, silver wire and a platinum wire were served as the working, reference and counter electrode, respectively. The film surface morphology was determined by atomic force microscopy (AFM) (Seiko Instruments, SPA-400).

2.2. Devices measurements and characterization

Before usage, the glass substrates coated with indium tin oxide (ITO) with a sheet resistance of 15 Ω per square and then sequentially cleaned in an ultrasonic bath with deionized water, acetone and ethanol for 15 min. A PEDOT:PSS layer (50 nm) was spin-coated onto the ITO surface and baked at 150 °C for 10 min to remove the residual water. Then, an EML with a thickness of about 40 nm was spin-coated from a filtered 10 mg ml^{-1} 1, 2-dichloroethane solution onto the PEDOT: PSS layer and annealed at 80 °C for 30 min to remove the residual solvent under N_2 atmosphere. Then, an electron-transport layer TPBi, a Cs_2CO_3 layer and an Al layer were deposited consecutively onto the spin-coated film in a vacuum chamber at ~4×10^{-4} Pa with the deposition rates of 1–2 Å s^{-1}, 0.1 Å s^{-1}, 6 Å s^{-1}, respectively. The emission area was 2×2 mm^{-2} controlled through a shadow mask. All the characterizations were performed at room temperature in ambient condition without encapsulation. The current density and luminance versus driving voltage curves and electroluminescence spectra were measured by a Keithley 2400s source meter and PR655 spectra colorimeter. External quantum efficiencies of the devices were calculated assuming a Lambertian emission distribution.

2.3. Materials

2.3.1. Synthesis of 4-(9H-carbazol-3-yl)-N, N-diphenylaniline (3TC)

3-bromo-9H-carbazole (492.21 mg, 2 mmol), N,N-diphenyl-4-(4,4,5,5-tetramethyl-1,3,2-dioxaborolan-2-yl)aniline (965.35 mg, 2.6 mmol), potassium carbonate (414.63 g, 3 mmol), terakis(triphenylphosphine)palladium (115.56 mg, 0.1 mmol) were dissolved in a mixture solution of tetrahydrofuran (15 ml) and water (5 ml) and refluxed under nitrogen at 80 °C for 12 h. Then, the mixture was extracted with dichloromethane and washed with water. The organic layer was dried over anhydrous $MgSO_4$ and the residue was purified on a silica gel column using petroleum ether/dichloromethane mixture (3:1, v/v) as eluent to afford the product as white powder (1180.6 mg, yield: 89%). ^{1}H NMR (600 MHz, DMSO-d_6): δ [ppm]: 11.29 (s, 1H), 8.40 (s, 1H), 8.18 (d, $J = 7.7$ Hz, 1H), 7.72–7.65 (m, 3H), 7.53 (d, $J = 8.4$ Hz, 1H), 7.49 (d, $J = 8.1$ Hz, 1H), 7.39 (t, $J = 7.2$ Hz, 1H), 7.35–7.30 (m, 4H), 7.17 (t, $J = 7.4$ Hz, 1H), 7.10 (d, $J = 8.6$ Hz, 2H), 7.06 (t, $J = 8.5$ Hz, 6H). ^{13}C NMR (150 MHz, $CDCl_3$) δ [ppm]: 147.7, 147.0, 140.1, 139.9, 138.7, 135.8, 129.2, 128.1, 125.8, 124.4, 124.1, 123.2, 122.9, 122.3, 120.5, 120.3, 119.6, 118.8, 110.6, 108.5. Found: C, 87.6; H, 5.7; N, 6.7%; molecular formula $C_{30}H_{22}N_2$ requires: C, 87.8; H, 5.4; N, 6.8%. MS (MALDI-TOF) [m/z]: calcd for $C_{30}H_{22}N_2$, 410.1783; found, 410.1455.

2.3.2. Synthesis of 4-(9H-carbazol-2-yl)-N, N-diphenylaniline (2TC)

2TC was prepared via the same procedure to that of **3TC** using 2-bromo-9H-carbazole instead of 3-bromo-9H-carbazole as white power (1190.5 mg, yield: 91%). ^{1}H NMR (600 MHz, DMSO-d_6): δ [ppm]: 11.28 (s, 1H), 8.15 (d, $J = 8.1$ Hz, 1H), 8.11 (d, $J = 7.7$ Hz, 1H), 7.73–7.65 (m, 3H), 7.49 (d, $J = 8.1$ Hz, 1H), 7.44 (dd, $J = 8.2$, 1.4 Hz, 1H), 7.40–7.30 (m, 5H), 7.19–7.04 (m, 9H). ^{13}C NMR (150 MHz, $CDCl_3$) δ [ppm]: 147.8, 146.5, 139.9, 138.7, 136.4, 132.5, 129.2, 127.9, 126.0, 125.1, 124.5, 124.2, 123.9, 123.5, 122.7, 120.4, 119.6, 118.4, 110.8, 110.7. Found: C, 88.0; H, 5.3; N, 6.7%; molecular formula $C_{30}H_{22}N_2$ requires: C, 87.8; H, 5.4; N, 6.8%. MS (MALDI-TOF) [m/z]: calcd for $C_{30}H_{22}N_2$, 410.1783; found, 410.6247.

2.3.3. Synthesis of (4-(9H-carbazol-9-yl)phenyl)(4-bromophenyl) methanone (BrPM-Cz)

Bis(4-bromophenyl)methanone (680.02 mg, 2 mmol), carbazole (334.4 mg, 2 mmol), $Pd(OAc)_2$ (8.98 mg, 0.04 mmol), $HP(t\text{-}Bu)_3BF_4$ (11.6 mg, 0.04 mmol), t-BuONa (288.3 mg, 1.3 mmol) were dissolved in 30 ml toluene refluxed for 24 h under nitrogen. After cooled, the mixture was extracted with dichloromethane and washed with brine for three times. After dried over anhydrous Na_2SO_4, the solvent was removed under reduced pressure and the residue was purified with column chromatography on silica gel using petroleum ether/dichloromethane mixture (5:1, v/v) as the eluent to afford the product as white powder

(857.3 mg, yield: 53%). ^{1}H NMR (600 MHz, DMSO-d_6): δ [ppm]: 8.15 (d, J = 7.8 Hz, 2H), 8.04 (d, J = 8.4 Hz, 2H), 7.78 (d, J = 8.5 Hz, 2H), 7.74 (d, J = 8.4 Hz, 2H), 7.69 (d, J = 8.5 Hz, 2H), 7.52 (d, J = 8.2 Hz, 2H), 7.47–7.42 (m, 2H), 7.33 (t, J = 7.4 Hz, 2H). ^{13}C NMR (150 MHz, $CDCl_3$) δ [ppm]: 194.5, 142.0, 140.2, 136.2, 135.5, 131.8, 131.8, 131.6, 127.8, 126.4, 126.3, 123.9, 120.7, 120.5, 109.8. Found: C, 70.8; H, 3.7; N, 3.4%; molecular formula $C_{25}H_{16}BrNO$ requires C, 70.4; H, 3.8; N, 3.3%. MS (MALDI-TOF) [m/z]: calcd for $C_{25}H_{16}BrNO$, 425.0415; found, 426.4393.

2.3.4. Synthesis of (4-(3-(4-(diphenylamino)phenyl)-9H-carbazol-9-yl)phenyl)(phenyl)methanone (3TCPM)

3TCPM was prepared via the same procedure to that of **BrPM-Cz** using (4-bromophenyl)(phenyl)methanone and **3 TC** instead of bis(4-bromophenyl)methanone and carbazole as green power (564.2 mg, yield: 84%). ^{1}H NMR (600 MHz, $CDCl_3$): δ [ppm]: 8.34 (s, 1H), 8.19 (d, J = 7.7 Hz, 1H), 8.10 (d, J = 8.5 Hz, 2H), 7.95–7.90 (m, 2H), 7.76 (d, J = 8.5 Hz, 2H), 7.68–7.64 (m, 2H), 7.61 (d, J = 8.6 Hz, 2H), 7.59–7.54 (m, 4H), 7.48–7.45 (m, 1H), 7.35 (t, J = 7.1 Hz, 1H), 7.29 (t, J = 7.9 Hz, 4H), 7.20 (d, J = 8.1 Hz, 2H), 7.17 (d, J = 7.8 Hz, 4H), 7.04 (t, J = 7.3 Hz, 2H). ^{13}C NMR (150 MHz, $CDCl_3$) δ [ppm]: 195.6, 147.8, 146.7, 141.7, 140.7, 139.5, 137.5, 136.0, 133.7, 132.7, 132.0, 130.1, 129.3, 128.5, 128.0, 126.4, 126.2, 125.4, 124.4, 124.4, 124.3, 124.0, 122.8, 120.8, 120.5, 118.5, 110.1, 110.0. Found: C, 87.5; H, 5.4; N, 4.3%; molecular formula $C_{43}H_{30}N_2O$ requires C, 87.4; H, 5.1; N, 4.7%. MS (MALDI-TOF) [m/z]: calcd for $C_{43}H_{30}N_2O$, 590.2358; found, 590.1614.

2.3.5. Synthesis of (4-(2-(4-(diphenylamino)phenyl)-9H-carbazol-9-yl)phenyl)(phenyl)methanone (2TCPM)

2TCPM was prepared via the same procedure to that of **BrPM-Cz** using (4-bromophenyl)(phenyl)methanone and **2 TC** instead of bis(4-bromophenyl)methanone and carbazole as green power (550.7 mg, yield: 82%). ^{1}H NMR (600 MHz, DMSO-d_6): δ [ppm]: 8.32 (d, J = 8.1 Hz, 1H), 8.28 (d, J = 7.7 Hz, 1H), 8.06 (d, J = 8.3 Hz, 2H), 7.92 (d, J = 8.3 Hz, 2H), 7.87 (d, J = 7.4 Hz, 2H), 7.72 (t, J = 7.4 Hz, 1H), 7.69 (s, 1H), 7.66 (d, J = 8.5 Hz, 2H), 7.62 (d, J = 7.7 Hz, 2H), 7.60 (d, J = 2.7 Hz, 1H), 7.55 (d, J = 8.2 Hz, 1H), 7.47 (t, J = 7.6 Hz, 1H), 7.36–7.30 (m, 5H), 7.08 (s, 1H), 7.07–7.03 (m, 7H). ^{13}C NMR (150 MHz, $CDCl_3$) δ [ppm]: 195.7, 147.7, 147.2, 141.7, 141.0, 140.8, 139.4, 137.5, 136.2, 135.7, 132.7, 132.0, 130.1, 129.3, 128.5, 128.2, 126.5, 126.1, 124.4, 124.0, 123.7, 123.0, 122.7, 120.8, 120.7, 120.5, 112.0, 109.8, 107.8. Found: C, 87.1; H, 5.5; N, 5.0%; molecular formula $C_{43}H_{30}N_2O$ requires C, 87.4; H, 5.1; N, 4.7%. MS (MALDI-TOF) [m/z]: calcd for $C_{43}H_{30}N_2O$, 590.2358; found, 590.1312.

2.3.6. Synthesis of (4-(1-(4-(diphenylamino)phenyl)-9H-carbazol-9-yl)phenyl)(phenyl)methanone (1TCPM)

1 TC (821.04 mg, 2 mmol), (4-bromophenyl)(phenyl)methanone (680.02 mg, 2 mmol), [1,1′-biphenyl]-2-yldicyclohexylphosphine (852.63 mg, 2 mmol), t-BuONa (288.3 mg, 3 mmol), and $Pd_2(dba)_3$ (36.63 mg, 0.04 mmol) were dissolved in 30 ml toluene and refluxed for 24 h under nitrogen. After cooled, the mixture was extracted with dichloromethane and washed with brine for three times. After dried over anhydrous Na_2SO_4, the solvent was removed under reduced pressure and the residue was purified with column chromatography on silica gel using petroleum ether/dichloromethane mixture (5:1, v/v) as the eluent to afford the product as green powder (705.5 mg, yield: 47%). ^{1}H NMR (600 MHz, $CDCl_3$): δ [ppm]: 1H NMR (600 MHz, CDCl3) δ 8.20–8.13 (m, 2H), 7.78 (d, J = 7.1 Hz, 2H), 7.75 (d, J = 8.4 Hz, 2H), 7.58 (t, J = 7.4 Hz, 1H), 7.45 (t, J = 7.8 Hz, 2H), 7.43–7.38 (m, 3H), 7.37–7.31 (m, 2H), 7.23 (d, J = 8.4 Hz, 2H), 7.22–7.17 (m, 4H), 6.98 (t, J = 8.1 Hz, 4H), 6.94 (d, J = 7.6 Hz, 4H), 6.76 (d, J = 8.5 Hz, 2H). ^{13}C NMR (150 MHz, $CDCl_3$) δ [ppm]: 195.4, 147.5, 146.5, 143.0, 142.0, 137.7, 137.7, 135.2, 132.8, 132.3, 130.7, 130.0, 129.9, 129.3, 128.9, 128.4, 127.5, 126.6, 126.3, 125.5, 124.7, 123.8, 123.1, 121.8, 120.8, 120.7, 120.3, 119.2, 110.0. Found: C, 87.1; H, 5.4; N, 5.0%; molecular formula $C_{43}H_{30}N_2O$ requires C, 87.4; H, 5.1; N, 4.7%. MS (MALDI-TOF) [m/z]: calcd for $C_{43}H_{30}N_2O$, 590.2358; found, 590.1807.

2.3.7. Synthesis of (4-(9H-carbazol-9-yl)phenyl)(4-(1-(4-(diphenylamino)phenyl)-9H-carbazol-9-yl)phenyl)methanone (1TCPM-Cz)

1TCPM-Cz was prepared via the same procedure to that of **1TCPM** using **BrPM-Cz** instead of (4-bromophenyl)(phenyl)methanone as green power (368.2 mg, yield: 44%). ^{1}H NMR (600 MHz, $CDCl_3$): δ [ppm]: 8.15–8.07 (m, 4H), 7.97 (d, J = 8.3 Hz, 2H), 7.78 (d, J = 8.3 Hz, 2H), 7.63 (d, J = 8.3 Hz, 2H), 7.43 (d, J = 8.2 Hz, 2H), 7.39–7.32 (m, 6H), 7.27 (dd, J = 14.5, 7.2 Hz, 3H), 7.23 (d, J = 8.3 Hz, 2H), 7.23 (d, J = 8.3 Hz, 2H), 7.10 (t, J = 7.8 Hz, 4H), 6.95 (d, J = 8.4 Hz, 2H), 6.93–6.85 (m, 6H), 6.72 (d, J = 8.4 Hz, 2H). ^{13}C NMR (150 MHz, $CDCl_3$) δ [ppm]: 194.3, 147.4, 146.4, 143.2, 141.9, 141.6, 140.3, 137.7, 136.0, 135.0, 132.9, 131.8, 130.6, 129.9, 129.3, 129.0, 127.6, 126.6, 126.4, 126.4, 126.2, 125.5, 124.5, 123.9, 123.8, 123.1, 122.1, 120.9, 120.8, 120.6, 120.5, 120.3, 119.2, 110.0, 109.8. Found: C, 87.1; H, 4.6; N, 5.9%; molecular formula $C_{55}H_{37}N_3O$ requires C, 87.4; H, 4.9; N, 5.6%. MS (MALDI-TOF) [m/z]: calcd for $C_{55}H_{37}N_3O$, 755.2937; found, 755.2093.

3. Result and discussion

The chemical structures and design strategy of the objective TADF emitters are presented in Fig. 1 and the synthetic strategy is shown in Scheme 1. The key intermediates of **3 TC** and **2 TC** were routinely synthesized by linking the triphenylamine unit with corresponding bromine-substituted carbazole moieties via Suzuki coupling reaction. The intermediate **1 TC** was synthesized according to previous literatures [26]. Then, these intermediates were reacted with the (4-bromophenyl)(phenyl)methanone by means of Buchwald-Hartwig reaction, affording the desired TADF emitters, namely: **3TCPM**, **2TCPM**, and **1TCPM**. Furthermore, **1TCPM-Cz** was designed by introducing an additional carbazole unit to the phenyl ketone for the purpose of increasing molecular rigidity and radiative efficiency. It could be speculated that the types of charge transfer process in these emitters could be regulated from the TBCT to TSCT due to the geometric restraint resulted from the relative position of donor and acceptor units. As well known, the concept of regioisomer is of significant in adjusting molecular properties in various application fields such as OLEDs, organic field-effect transistors (OFETs), and organic photovoltaic (OPVs) [33–37]. Therefore, the impact of regioisomers on the electroluminescence properties are also investigated using the regioisomeric compounds of **3TCPM**, **2TCPM**,

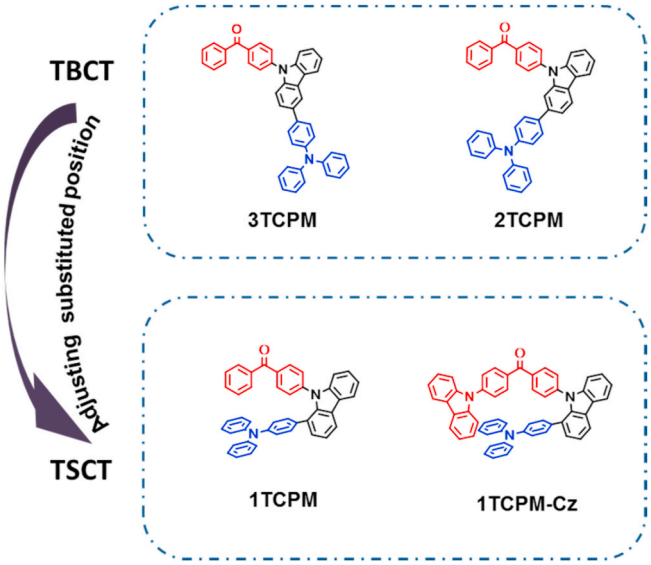

Fig. 1. Molecular structures and design strategy of the targeted TADF emitters.

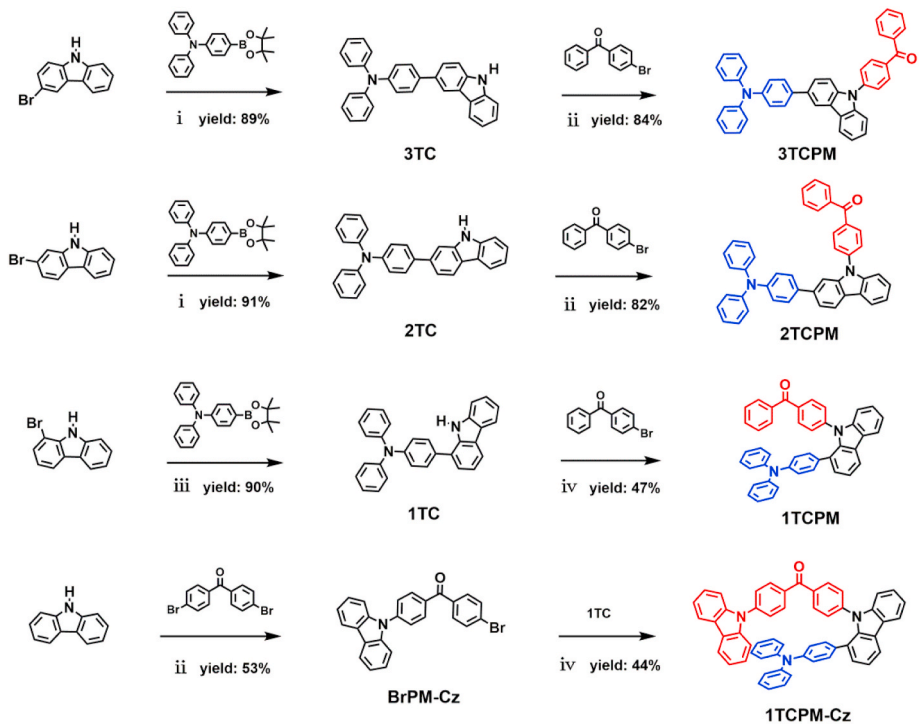

Scheme 1. Synthetic routes of the TADF emitters: (i) $Pd(PPh_3)_4$, K_2CO_3, THF, H_2O, 80 °C; (ii) $Pd(OAc)_2$, $HP(t\text{-}Bu)_3BF_4$, t-BuONa, toluene, reflux; (iii) Pd2(dba)3, K2CO3, P(t-Bu)3, reflux; (iv) [1,1′-biphenyl]-2-yldicyclohexylphosphine, t-BuONa, $Pd_2(dba)_3$, toluene, reflux.

and **1TCPM**. These TADF materials were purified through silica gel column chromatography, followed by recrystallization before measurements and device fabrication processes. The molecular structures were fully confirmed by ^{1}H and ^{13}C NMR spectroscopies, elemental analyses and matrix-assisted laser desorptionionization time-of-flight mass spectrometry (MALDI-TOF-MS).

3.1. Theoretical calculations

To better comprehend the relationship between the molecular spatial structures and photophysical properties of the four emitters at molecular level, geometry configuration and frontier molecular orbitals were conducted employing density functional theory (DFT) calculation under the level of B3LYP/6-31G (d). The frequency calculations have been performed to ensure that the optimized geometry is a minimum. As shown in Fig. 2, in the optimized molecular structures, the dihedral angles between the carbazole bridge and triphenylamine was 58.16° and 53.20° for **1TCPM** and **1TCPM-Cz**, respectively, which were larger than that of **3TCPM** and **2TCPM** (35.14° and 34.55°, respectively). The highly twisted configuration of **1TCPM** and **1TCPM-Cz** could be attributed to the huge steric hindrance between donor and acceptor and will lead to increased electron interaction of them.

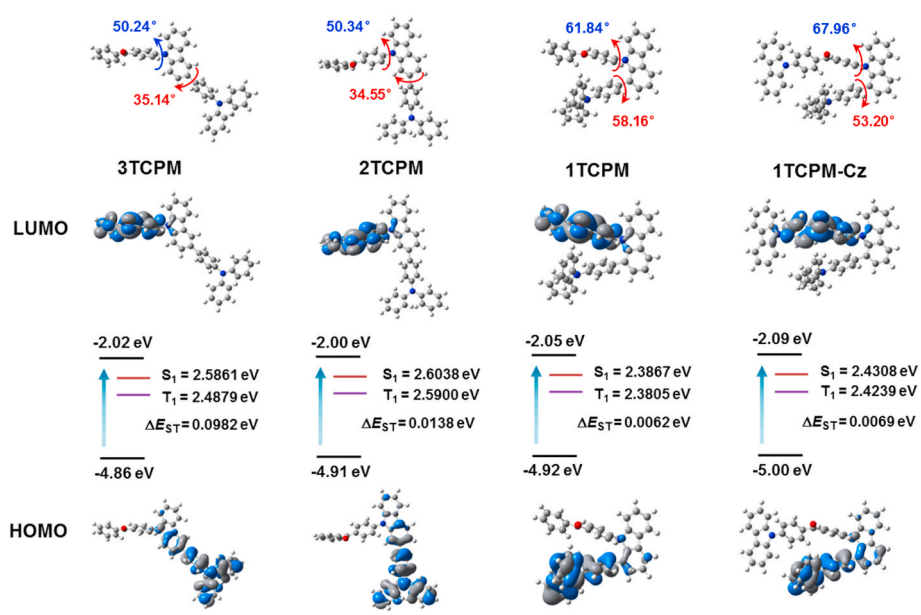

Fig. 2. The optimized molecular structures, HOMO/LUMO distributions and their singlet/triplet splitting (ΔE_{ST}) of these emitters.

The HOMOs of these emitters were all distributed on the triphenylamine groups due to the stronger electron-donating ability, and the LUMOs mainly located on the phenyl ketone group resulted from the electron-deficient property. Accordingly, it could be speculated that charge transfer of **3TCPM** occurred mainly through bond due to the directly linking of donor and acceptor. As for **1TCPM** and **1TCPM-Cz**, TSCT of the spatially close donor and acceptor could be anticipated. These emitters possessed the similar LUMO levels of −2.00 eV to −2.09 eV due to the acceptors were all phenyl ketone. Based on the time-dependent density functional theory (TD-DFT) calculations using diffuse functions of 6-31G + (d), the ΔE_{ST} were computed. Thanks to the HOMO and LUMO distributions of **1TCPM** and **1TCPM-Cz** were commendably separated, smaller ΔE_{ST} values (0.0062 eV and 0.0069 eV, respectively) could be expected, which was smaller than that of **3TCPM** and **2TCPM** (0.0982 eV and 0.0138 eV, respectively). The very small ΔE_{ST} values made **1TCPM** and **1TCPM-Cz** promising TADF candidates by promoting RISC. Moreover, as presented in Fig. S9, the ortho-positioned triphenylamine units showed a close proximity with the acceptor units with the distance of 3.22–3.68 Å in **1TCPM** and 3.21–4.51 Å in **1TCPM-Cz**, indicating the possibility of charge transfer through space existed. Besides, the HOMO-1 of these emitters was situated at the carbazole units, which was favorable to the carrier injection, transport and recombination processes [38]. The first singlet and triplet excited states were further analyzed by natural transition orbitals (NTOs) and given in Fig. S5, the holes of the emitters were mainly localized at the triphenylamine and partly expanded to carbazole bridge, and the particles were situated at phenyl ketone, suggesting a predominant charge transfer of these emitters, which was consistent with the fluorescence and phosphorescence spectra. Furthermore, the spin density of triplet states of the emitters were calculated and presented in Fig. S7. The calculated spin densities of the triplet states were mainly distributed on the phenyl ketone moieties and slightly distributed on the donor part. Therefore, the spatially close donor in TSCT emitters could prevent the interaction of triplets between neighbouring molecules more effective in solid states, benefiting to alleviate triplet-triplet annihilation.

3.2. Photophysical properties

The UV–vis absorptions of the emitters in toluene were presented in Fig. 3. The higher energy absorptions from 290 to 320 nm were stemmed from the π-π* transitions of the conjugated aromatic skeleton, and the low energy absorption band at 350 nm can be attributed to the ICT transition. From the fluorescence spectra in toluene, **2TCPM**, **1TCPM**, and **1TCPM-Cz** displayed dual emissions, which could attributed to the local excitation (LE) states of the donor or acceptor and CT states emission from the donor-acceptor charge transfer [25]. The emissions in various solvents with different polarity were further investigated. As shown in Fig. S1, with the increased polarity, the CT states emission of **2TCPM**, **1TCPM**, and **1TCPM-Cz** exhibited obvious bathochromic shifts, while only slight change of emission peaks from LE states could be observed, which confirmed the dual emissions were from LE and CT states. The TSCT emitters of **1TCPM**, and **1TCPM-Cz** expressed intense and single emissions in neat films at room temperature, demonstrating favorable donor-acceptor combination in solid state. The phosphorescence spectra measured in neat films at 77 K were shown in Fig. 4. The S_1/T_1 energy levels were 2.71/2.55, 2.81/2.44, 2.78/2.76 and 2.75/2.71 eV of **3TCPM**, **2TCPM**, **1TCPM**, and **1TCPM-Cz**, respectively. Therefore, the ΔE_{ST} was calculated to be 0.26, 0.37, 0.02 and 0.04 eV for **3TCPM**, **2TCPM**, **1TCPM**, and **1TCPM-Cz**, respectively. It is noteworthy that the ΔE_{ST} of **1TCPM** and **1TCPM-Cz** were narrower than that of **3TCPM** and **2TCPM**, resulting from the fortified separation of HOMO and LUMO and beneficial for more effective RISC from triplet to singlet states (see Table 1).

For the aim of notarizing TADF behaviors, the transient PL decay curves in neat films were performed under N_2 atmosphere. The decays of the emitters presented in Fig. 3 (d) were bi-exponential which involving prompt and delayed components. The summarized data of prompt and delayed lifetimes were displayed in Table 2. The short lifetime components of these emitters (13.1–21.2 ns) could be attributed to the conventional fluorescence. Their long-delayed components (1.6–2.3 μs) were caused by the transition of delayed S_1 from the non-radiative T_1 state via the reverse intersystem. For further confirming TADF feature, the transient PL decay curves of the emitters were measured in toluene solution under N_2 and air, respectively (Fig. S4). The increased delayed components under N_2 in comparison with air implied that the emitters

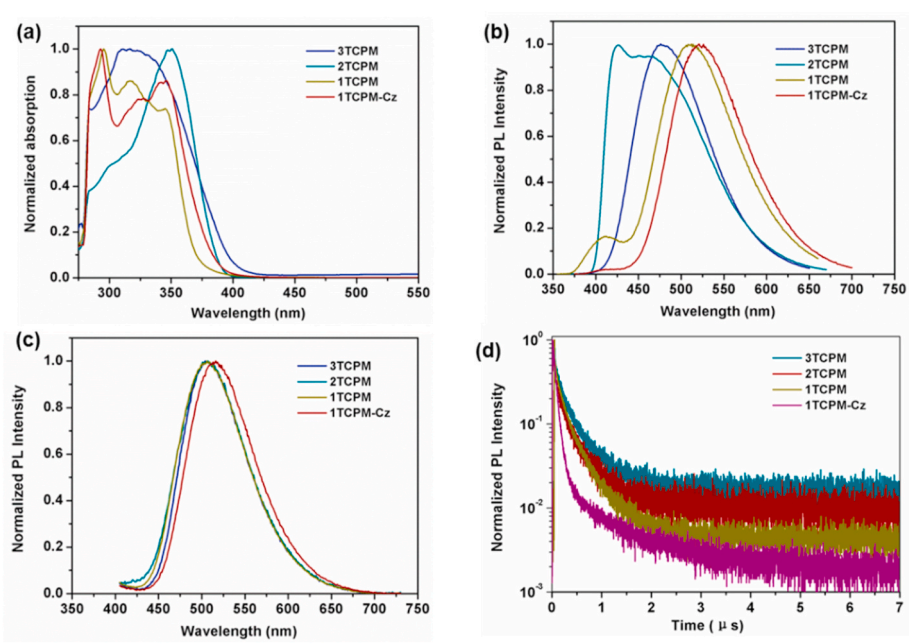

Fig. 3. The UV–vis absorptions (a) and fluorescence spectra (b) of these emitters measured in toluene solution (10^{-5} M). (c) The fluorescence spectra in neat film states. (d) The transient PL decay spectra in neat film states at room temperature under N_2 atmosphere.

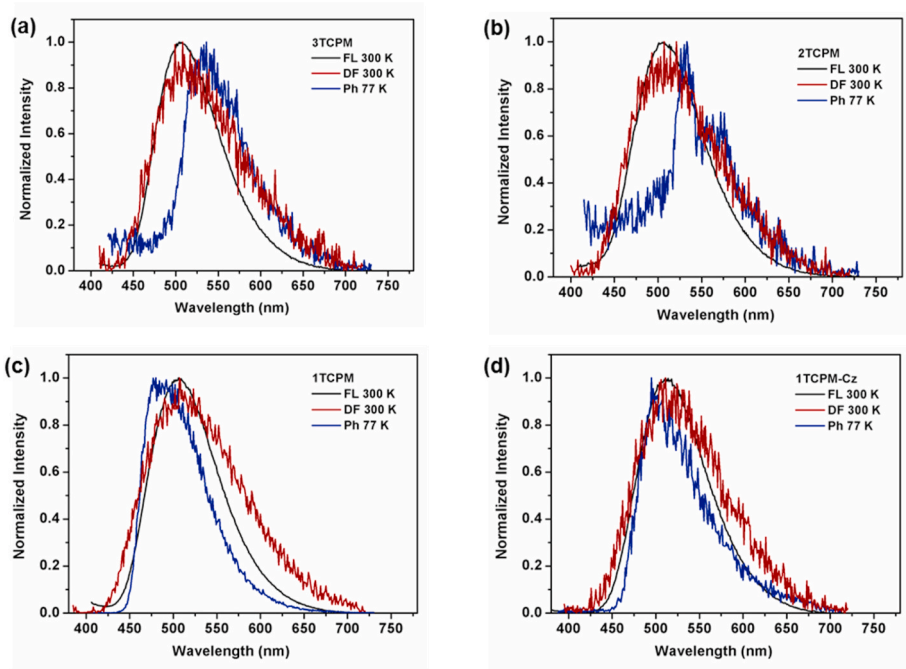

Fig. 4. The FL, DF, and Ph of these TADF emitters measured in neat film states at 300 K and 77 K, respectively.

Table 1
Photophysical and electrochemical parameters of these TADF emitters.

Compound	T_d[a]/T_g[a] [°C]	λ_{abs}[b] [nm]	λ_{em}[c] [nm]	E_g[d] [eV]	HOMO[e] [eV]	LUMO[f] [eV]	S_1[g]/T_1[h] [eV]	ΔE_{ST}[i] [eV]
3TCPM	367/-	335	478	2.39	−5.55	3.16	2.81/2.55	0.26
2TCPM	377/148	350	425, 464	2.43	−5.58	3.15	2.81/2.44	0.37
1TCPM	407/-	345	411, 510	2.33	−5.51	3.18	2.78/2.76	0.02
1TCPM-Cz	433/-	346	411, 521	2.30	−5.36	3.06	2.75/2.71	0.04

[a]T_d and T_g were measured by TGA and DSC. [b]Measured in toluene solution (10^{-5} M). [c]Measured in toluene solution (10^{-5} M). [d]Estimated from the absorption onset. [e]Determined from the cyclic voltammograms. The oxidation potential of Fc/Fc^+ was measured to be 0.35 eV. HOMO = $-(4.8 + E^{OX}_{onset} - 0.35)$ eV. [f]LUMO = HOMO + E_g. [g]Determined from the onset of the fluorescence spectra in neat films at 300 K. [h]Obtained at 77 K in neat films. [i]Splitting between S_1 and T_1 energy.

Table 2
Photophysical characteristics and kinetic parameters of the TADF emitters in neat film states.

Emitter	φ_{PL}[a] [%]	φ_p[b] [%]	φ_d[b] [%]	τ_p[c] [ns]	τ_d[c] [μs]	$k_{r,S}$[d] [10^7 s^{-1}]	$k_{nr,S}$[d] [10^6 s^{-1}]	k_{ISC}[d] [10^7 s^{-1}]	k_{RISC}[d] [10^6 s^{-1}]
3TCPM	35	16	19	19.7	2.1	0.81	1.48	2.80	1.05
2TCPM	20	9	11	21.2	2.3	0.43	1.74	2.45	0.94
1TCPM	50	13	38	14.2	1.7	0.89	0.87	5.95	2.34
1TCPM-Cz	57	12	45	13.1	1.6	0.92	0.69	5.99	2.97

[a]Measured in neat films using integrating sphere under N_2. [b]Φ_p and Φ_d are the prompt fluorescence and delayed fluorescence quantum yield, respectively; τ_p and τ_d are the lifetimes of the prompt and delayed decay components, respectively. [d]$k_{r,S}$, $k_{nr,S}$, k_{ISC} and k_{RISC} are the rate constant for fluorescence radiative transition, non-radiative transition, intersystem crossing (ISC) and reverse intersystem crossing (RISC) processes, respectively.

had TADF feature. These results confirmed that all the emitters had TADF feature. Moreover, Fig. 4 gave the time-resolved photoluminescence spectra measured in neat film state under N_2 at 300 K. The observed similar shape of photoluminescence spectra before and after applying delay time (0.001 ms) manifesting that the delayed emission stemmed from the S_1 states through reversed process [39,40].

To further investigate the exciton utilization, the PLQYs of these emitters in solid states were obtained. The PLQYs of **1TCPM** and **1TCPM-Cz** were measured to be 50% and 57%, respectively, which was higher than that of **3TCPM** and **2TCPM** with the values of 35% and 20%, respectively. Further, the kinetic parameters were analyzed and summarized in Table 2. Although the $k_{r,S}$ values of **1TCPM** and **1TCPM-Cz** were similar with **3TCPM**, however, their $k_{nr,S}$ values were decreased obviously, suggesting the effectively suppressed non-radiative transition resulted from strong intramolecular interactions. Meanwhile, **1TCPM** and **1TCPM-Cz** possessed higher k_{RISC} values in comparison with **3TCPM**, which could ascribed for their very small ΔE_{ST} after transforming the charge transfer process from the TBCT to TSCT.

To investigate the aggregation-induced emission (AIE) characteristics, the PL behaviors of these emitters were performed to survey the emission intensity variation in THF/water mixed solvents at various water fractions. As shown in Fig. 5 (a) and (b) and S3, **1TCPM-Cz** exhibited a weak emission in a pure THF solution. Upon increasing the water fractions to 30%, a decrease of emission intensity was observed

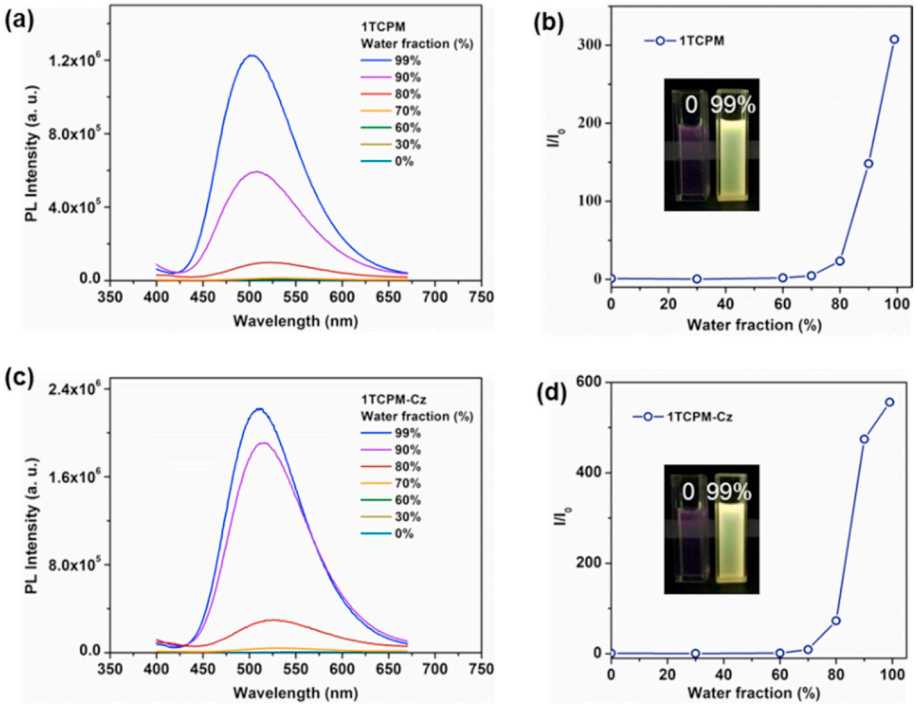

Fig. 5. PL spectra of **1TCPM** (a) and **1TCPM-Cz** (c) in THF/water mixtures at different water fractions. Plots of I/I_0 values versus water fractions of **1TCPM** (b) and **1TCPM-Cz** (d). I_0 is the PL intensity in pure THF solvent. Inset: photos of the emitters in corresponding THF/water mixtures under 365 nm excitation.

with a bathochromic-shift, owing to the dark twisted intramolecular charge transfer (TICT) state [41]. However, further increase of the water fractions to 99%, the emission became much stronger with a slight blue-shifted emission. The PL spectra of other emitters were also performed upon increasing the water fraction from 0% to 99% and a similar behavior could be observed. The PLQYs values in pure THF solution of **3TCPM** was 4%, and that of **2TCPM**, **1TCPM** and **1TCPM-Cz** were below 1%, which was lower than the values (**3TCPM**, **2TCPM**, **1TCPM** and **1TCPM-Cz** were measured to be 16%, 29%, 47% and 53%, respectively) obtained in mixed solution (THF/water 99%). These results clearly indicated that all emitters featured typical AIE characteristics [42,43]. Further, the α_{AIE} of **1TCPM** and **1TCPM-Cz** were determined to be 307 and 556, respectively, which was higher than that of **3TCPM** and **2TCPM** with the values of 193 and 130, respectively [44]. On one hand, the increased emission intensity could attribute to the intramolecular rotation requisite for the formation of a TICT state was obstructive after molecular aggregation. On the other hand, compared with **3TCPM** and **2TCPM**, the enhanced AIE effect of **1TCPM** and **1TCPM-Cz** could be ascribed to the strongly suppressed non-radiative decay resulted from both highly twisted structures and restricted intramolecular motion between the donor and acceptor [45].

3.3. Thermal properties

Thermogravimetric analyzer (TGA) and differential scanning calorimeter (DSC) were performed to explore the thermal stability of these emitters and presented in Fig. 6. All the emitters exhibited high decomposition temperatures (T_d, the temperature corresponding to 5% weight loss of the initial weight) around 367–433 °C. Furthermore, higher T_d with slightly increased values of the TSCT emitters of **1TCPM** and **1TCPM-Cz** could be observed in comparison with TBCT emitters of **3TCPM** and **2TCPM**, suggesting that incorporating TSCT could enhance the molecular rigidity. Meanwhile, except **2TCPM** displayed a high glass transition temperature (T_g) at 148 °C, no obvious T_g could be detected from 30 to 200 °C for **3TCPM**, **1TCPM**, and **1TCPM-Cz**. The improved thermal stability would benefit device stability during the solution process.

3.4. Electrochemical properties

For the sake of getting the frontier orbital energy levels, the electrochemical behaviors of these emitters were measured using cyclic voltammetry (CV) and plotted in Fig. 7. Two consecutive oxidation

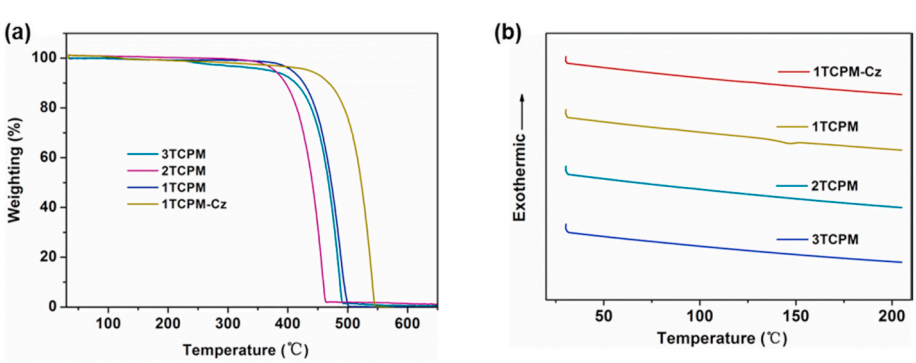

Fig. 6. TGA (a) and DSC (b) curves of these emitters at a heating rate of 10 °C min^{-1} under N_2.

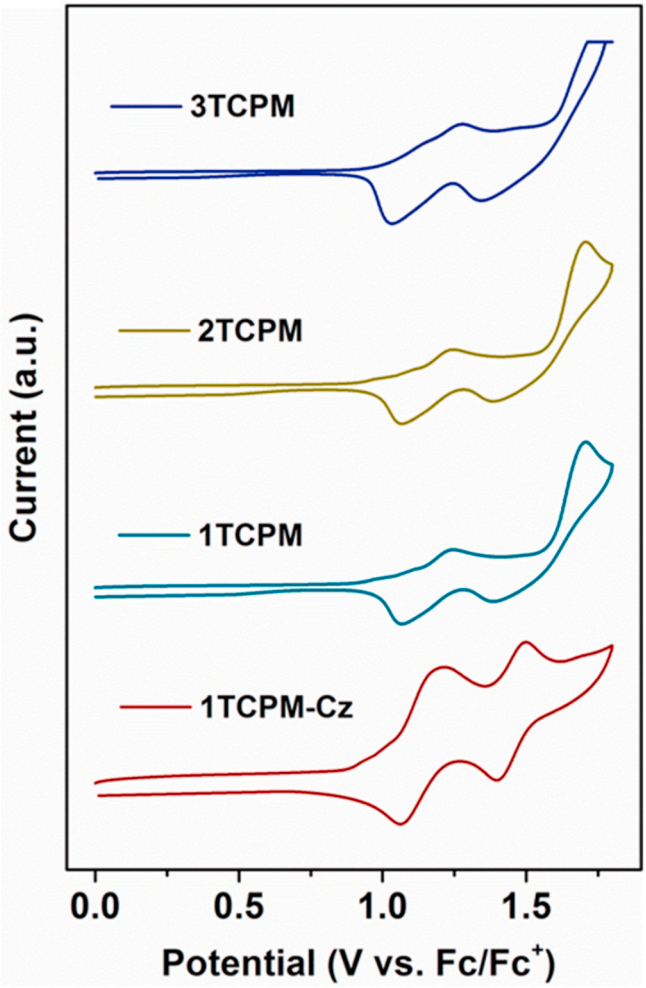

Fig. 7. Cyclic voltammetry (CV) of these emitters.

waves in CH_2Cl_2 could be observed with peak potentials at 1.20 V and 1.49 V of **1TCPM-Cz** and 1.24 V and 1.70 V for **1TCPM**. **3TCPM** and **2TCPM** also displayed two oxidation waves with the peaks at 1.27 V and 1.73 V, 1.25 V and 1.70 V, respectively. The potential for the first oxidation peak of **1TCPM-Cz** was lower than that of other emitters, demonstrating an easier oxidation process of **1TCPM-Cz**. The HOMO energy level should be determined by their respective onset of the first oxidation peak of front scan (1.10 V, 1.13 V, 1.06 V and 0.91 V for **3TCPM**, **2TCPM**, **1TCPM** and **1TCPM-Cz**, respectively). The HOMO energy levels of **3TCPM**, **2TCPM**, **1TCPM**, and **1TCPM-Cz** were estimated to be −5.55 eV, −5.58 eV, −5.51 eV, and −5.36 eV respectively, according to the onset potentials. The LUMO energy levels were found to be −3.16 eV, −3.15 eV, −3.18 eV and −3.06 eV for **3TCPM**, **2TCPM**, **1TCPM**, and **1TCPM-Cz**, respectively, which were calculated from the HOMO and optical band gap (E_g).

3.5. Properties for solution processing

Solution process abilities and film-forming ability closely relevant to the solubility of emitters in common solvents such as 1,2-dichloroethane, CH_2Cl_2, $CHCl_3$, and THF. The emitters exhibited superior solubility in these solvents, making them suitable for constructing solution-processed OLEDs. For better understanding the film-forming ability of the emitter (20 wt%) doped CzAcSF films, the surface morphologies of the blended films deposited by spin-coating were investigated by atomic force microscopy (AFM). As presented in Fig. 8, the tiny root-mean-square (RMS) roughness within the range of 0.311–0.372 nm, indicative of the prepared films were smooth and uniform. Besides, no significant particle aggregation or phase separation occurred in the blended films and the favorable morphology of the films further confirmed that these emitters were suitable for solution process [46].

3.6. Electroluminescence properties

Solution-processed devices were fabricated to explore the EL performance of these TADF molecules. The architecture was ITO/PEDOT:PSS (40 nm)/EML (40 nm)/TPBi (30 nm)/Cs_2CO_3 (2 nm)/Al (100 nm), in which poly(3,4-ethylenedioxythiophene):poly(styrenesulfonate) (PEDOT: PSS) and Cs_2CO_3 were hole- and electron-injection layers (HIL and EIL), and 1,3,5-tris(1-phenyl-1H-benzo[d]imidazole-2-yl)benzene (TPBi) was employed as an electron transporting layer (ETL). The emission layers were prepared with these AIE-active TADF emitters spin-coated films.

Based on the previous literatures, in the TADF-sensitized OLEDs, the T_1 excitons could be transited to S_1 through RISC and then transferred from the host to the guest by Förster energy transfer (FET) process, showing improved device efficiency than that of traditional host [47, 48]. Inspired by the advantages of TADF host, a bipolar blue TADF molecule of CzAcSF with high triplet energy level (3.04 eV) was selected as the host to fabricate devices and guarantee the T_1 excitons into the guests effectively [49]. The TADF emitters of **3TCPM**, **2TCPM**, **1TCPM**, and **1TCPM-Cz** were doped into the CzAcSF host with the optimized doping concentration of 20 wt%. The device architectures and performances of the solution-processed OLEDs were displayed in Fig. 9 and the detailed EL parameters were presented in Table 3. The EL spectra of these AIE-active TADF emitters based devices originated exclusively from the EML without emission from the adjacent layers, testifying the complete charge recombination in EML without any energy leakage. The TSCT emitter **1TCPM-Cz**-based device exhibited a green EL (505 nm) with the Commission Internationale de L'Eclairage coordinates of (0.29, 0.48), and a maximum CE of 35.5 cd A^{-1} and EQE of 13.3%, respectively. In consistence with the luminescence efficiency, TSCT emitter **1TCPM**-based device displayed relatively lower maximum CE and EQE of 17.9 cd A^{-1} and 7.6%, respectively, with the Commission Internationale de L'Eclairage coordinates of (0.26, 0.42). Conversely, the devices based on TBCT emitters of **3TCPM** and **1TCPM** showed relatively inferior efficiency with the maximum CE of 8.0 cd A^{-1} and 3.9 cd A^{-1}, as well as the EQE of 3.4% and 1.8%, respectively. In view of the relatively high luminescence efficiency of **3TCPM** and **1TCPM** in neat films, the non-doped devices employing the emitters were further fabricated with the same configuration (Fig. S10 and Table S1). The devices based on TBCT emitters of **1TCPM-Cz** and **1TCPM** exhibited maximum EQE of 3.7% and 2.3%, respectively, which was also better than that of TSCT emitters. The improved EL performance of TSCT-based TADF emitters could be explained by the following reasons. On one hand, own to the very small ΔEST , faster RISC realized, and therefore the ability of harvesting triplet excitons and converting them to singlet excitons for radiation of **1TCPM-Cz** and **1TCPM** were improved efficaciously in EL process. On another hand, the non-radiative decay could be restricted effectively own to the stronger intramolecular interaction and limited intramolecular motion. The results further demonstrated the feasibility of exploring high-performance TSCT TADF emitters by transforming the charge transfer from through bond to through space via regulating the conformation of donor and acceptor.

4. Conclusion

In this work, a series of AIE-active TADF emitters adopting triphenylamine as donor and phenyl ketone as acceptor unit were designed and developed. Via controlling the position of the donor and acceptor, the evolution of charge transfer category from through-bond to through-space was achieved. By virtue of the narrower ΔE_{ST} induced by valid separation of donor and acceptor, the reverse intersystem crossing

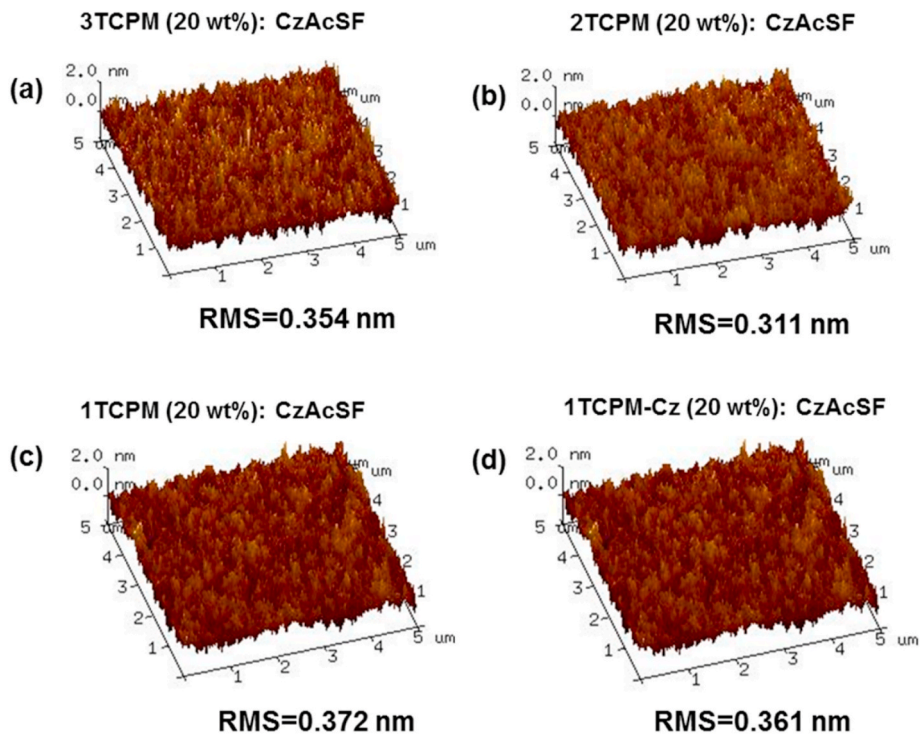

Fig. 8. AFM topographic images of the solution-processed doped films of the emitters (20 wt%) in CzAcSF.

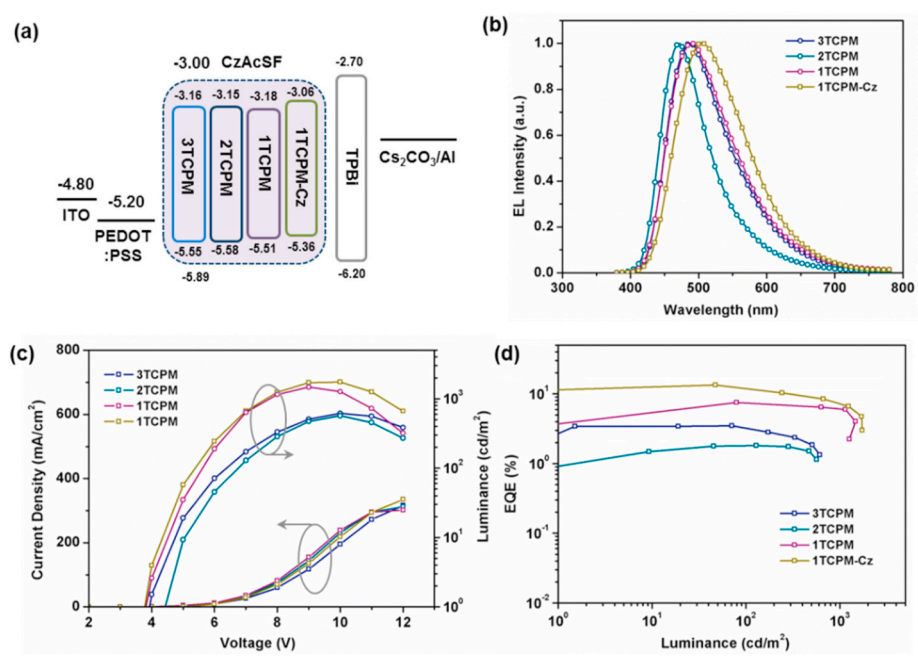

Fig. 9. (a) Energy diagram of the materials used in the solution-processed devices; (b) normalized EL spectral; (c) current density-voltage-luminance (J-V-L) curves; (d) EQE versus luminance curves.

(RISC) rate improved obviously, meanwhile, the restricted intramolecular motion suppresses the non-radiative decay effectively, resulting in improved luminescence efficiency. Furthermore, in comparison with TBCT emitters, the TSCT displayed enhanced AIE properties due to the strongly suppressed non-radiative decay resulted from both highly twisted structures and restricted intramolecular motion between donor and the acceptor. Consequently, solution-processed OLEDs based on TSCT emitter of **1TCPM-Cz** achieve a maximum CE of 35.5 cd A^{-1} and EQE of 13.3%, respectively, with a bipolar blue TADF material as host, displaying higher performance than TBCT analogues. The work provides a convenient design manner to realize high-performance TSCT-type emitters via regulating the conformation of the donor and acceptor.

Author Statement

Fulong Ma synthesized the molecules in the article, performed measurements, data analysis, devices measurements and

Table 3
Electroluminescence characteristics of the solution-processed devices.

Device	λ_{em} [nm]	V_{on}[a] [V]	CE_{max}[b] [Cd A^{-1}]	L_{max}[c] [cd m^{-1}]	EQE_{max}[d] [%]	PE_{max}[e] [lm W^{-1}]	CIE[f] (x, y)
3TCPM	487	3.9	8.0	615	3.4	4.2	(0.27, 0.43)
2TCPM	471	4.4	3.9	568	1.8	1.7	(0.21, 0.29)
1TCPM	489	3.8	17.9	1472	7.6	11.2	(0.26, 0.42)
1TCPM-Cz	505	3.8	35.5	1738	13.3	22.3	(0.29, 0.48)

[a] Turn-on voltage measured at 1 cd m^{-2}.
[b] CEmax = maximum current efficiency.
[c] L_{max} = maximum luminance.
[d] EQEmax = maximum external quantum efficiency.
[e] PEmax = maximum power efficiency.
[f] Commission International de I'Eclairage coordinates at 1 cd m^{-2}.

characterization and wrote. Hefang Ji executed the theoretical calculation and analysis. Dongdong Zhang carried out the tests of electrochemical behaviors. Ke Xue participate in the preparation of molecules. Pan Zhang performed the fluorescence spectra. Zhengjian Qi reviewed and modified the article. Huaiyuan Zhu reviewed and edited the article.

Declaration of competing interest

The authors declare that they have no known competing financial interests or personal relationships that could have appeared to influence the work reported in this paper.

Acknowledgements

The authors gratefully acknowledge the supporting from the Ministry of Science and Technology key research and development plan (2018YFF0215204) and the Science and Technology Achievements Transformation Special Fund of Jiangsu Province (BA2019052).

Appendix A. Supplementary data

Supplementary data to this article can be found online at https://doi.org/10.1016/j.dyepig.2021.109208.

References

[1] Uoyama H, Goushi K, Shizu K, Nomura H, Adachi C. Highly efficient organic light-emitting diodes from delayed fluorescence. Nature 2012;492(7428):234–8.
[2] Ahn DH, Kim SW, Lee H, Ko IJ, Karthik D, Lee JY, et al. Highly efficient blue thermally activated delayed fluorescence emitters based on symmetrical and rigid oxygen-bridged boron acceptors. Nat Photon 2019;13(8):540–6.
[3] Goushi K, Yoshida K, Sato K, Adachi C. Organic light-emitting diodes employing efficient reverse intersystem crossing for triplet-to-singlet state conversion. Nat Photon 2012;6(4):253–8.
[4] Rajamalli P, Senthilkumar N, Huang PY, Ren-Wu CC, Lin HW, Cheng CH. New molecular design concurrently providing superior pure blue, thermally activated delayed fluorescence and optical out-coupling efficiencies. J Am Chem Soc 2017;139(32):10948–51.
[5] Wu K, Zhang T, Wang Z, Wang L, Zhan L, Gong S, et al. De Novo Design of excited-state intramolecular proton transfer emitters via a thermally activated delayed fluorescence channel. J Am Chem Soc 2018;140(28):8877–86.
[6] Zhang Q, Li J, Shizu K, Huang S, Hirata S, Miyazaki H, et al. Design of efficient thermally activated delayed fluorescence materials for pure blue organic light emitting diodes. J Am Chem Soc 2012;134(36):14706–9.
[7] Albrecht K, Matsuoka K, Fujita K, Yamamoto K. Carbazole dendrimers as solution-processable thermally activated delayed-fluorescence materials. In: Chem Int Angew, editor54; 2015. p. 5677–82. 19.
[8] Chen JX, Tao WW, Chen WC, Xiao YF, Wang K, Cao C, et al. Red/near-infrared thermally activated delayed fluorescence oleds with near 100 % internal quantum efficiency. In: Chem Int Angew, editor58; 2019. p. 14660–5. 41.
[9] Wang K, Zheng CJ, Liu W, Liang K, Shi YZ, Tao SL, et al. Avoiding energy loss on tadf emitters: controlling the dual conformations of D-A structure molecules based on the pseudoplanar segments. Adv Mater 2017;47:29.
[10] Zhang D, Song X, Gillett AJ, Drummond BH, Jones STE, Li G, et al. Efficient and stable deep-blue fluorescent organic light-emitting diodes employing a sensitizer with fast triplet upconversion. Adv Mater 2020;32(19):1908355.
[11] Cai X, Li X, Xie G, He Z, Gao K, Liu K, et al. "Rate-limited effect" of reverse intersystem crossing process: the key for tuning thermally activated delayed fluorescence lifetime and efficiency roll-off of organic light emitting diodes. Chem Sci 2016;7(7):4264–75.
[12] Huang Z, Bin Z, Su R, Yang F, Lan J, You J. Molecular design of non-doped oleds based on a twisted heptagonal acceptor: a delicate balance between rigidity and rotatability. Angew Chem Int Ed 2020;59(25):9992–6.
[13] Lee SY, Yasuda T, Yang YS, Zhang Q, Adachi C. Luminous butterflies: efficient exciton harvesting by benzophenone derivatives for full-color delayed fluorescence OLEDs. Angew Chem Int Ed. 2014;53(25):6402–6.
[14] Shi YZ, Wang K, Li X, Dai GL, Liu W, Ke K, et al. Intermolecular charge-transfer transition emitter showing thermally activated delayed fluorescence for efficient non-doped OLEDs. Angew Chem Int Ed 2018;57(30):9480–4.
[15] Cho YJ, Jeon SK, Chin BD, Yu E, Lee JY. The design of dual emitting cores for green thermally activated delayed fluorescent materials. Angew Chem Int Ed 2015;54(17):5201–4.
[16] Zheng X, Huang R, Zhong C, Xie G, Ning W, Huang M, et al. Achieving 21% external quantum efficiency for nondoped solution-processed sky-blue thermally activated delayed fluorescence oleds by means of multi-(donor/acceptor) emitter with through-space/-bond charge transfer. Adv Sci 2020;7(7):1902087.
[17] Yang SY, Wang YK, Peng CC, Wu ZG, Yuan S, Yu YJ, et al. Circularly polarized thermally activated delayed fluorescence emitters in through-space charge transfer on asymmetric spiro skeletons. J Am Chem Soc 2020;142(41):17756–65.
[18] Tang X, Cui LS, Li HC, Gillett AJ, Auras F, Qu YK, et al. Highly efficient luminescence from space-confined charge-transfer emitters. Nat Mater 2020;19(12):1332–8.
[19] Lin TA, Chatterjee T, Tsai WL, Lee WK, Wu MJ, Jiao M, et al. Sky-blue organic light emitting diode with 37% external quantum efficiency using thermally activated delayed fluorescence from spiroacridine-triazine hybrid. Adv Mater 2016;28(32):6976–83.
[20] Wada Y, Kubo S, Kaji H. Adamantyl substitution strategy for realizing solution-processable thermally stable deep-blue thermally activated delayed fluorescence materials. Adv Mater 2018;30(8):1705641.
[21] Zeng W, Lai HY, Lee WK, Jiao M, Shiu YJ, Zhong C, et al. Achieving nearly 30% external quantum efficiency for orange-red organic light emitting diodes by employing thermally activated delayed fluorescence emitters composed of 1,8-naphthalimide-acridine hybrids. Adv Mater 2018;30(5):1704961.
[22] Chen JX, Wang K, Zheng CJ, Zhang M, Shi YZ, Tao SL, et al. Red organic light-emitting diode with external quantum efficiency beyond 20% based on a novel thermally activated delayed fluorescence emitter. Adv Sci 2018;5(9):1800436.
[23] Ban X, Zhu A, Zhang T, Tong Z, Jiang W, Sun Y. Highly efficient all-solution-processed fluorescent organic light-emitting diodes based on a novel self-host thermally activated delayed fluorescence emitter. ACS Appl Mater Interfaces 2017;9(26):21900–8.
[24] Peng CC, Yang SY, Li HC, Xie GH, Cui LS, Zou SN, et al. Highly efficient thermally activated delayed fluorescence via an unconjugated donor-acceptor system realizing EQE of over 30%. Adv Mater 2020;32(48):2003885.
[25] Lv X, Wang Y, Li N, Cao X, Xie G, Huang H, et al. Regulating the photophysical properties of highly twisted TADF emitters by concurrent through-space/-bond charge transfer. Chem Eng J 2020;402:126173.
[26] Lin J-A, Li S-W, Liu Z-Y, Chen D-G, Huang C-Y, Wei Y-C, et al. Bending-type electron donor–donor–acceptor triad: dual excited-state charge-transfer coupled structural relaxation. Chem Mater 2019;31(15):5981–92.
[27] Hu J, Li Q, Wang X, Shao S, Wang L, Jing X, et al. Developing Through-space charge transfer polymers as a general approach to realize full-color and white emission with thermally activated delayed fluorescence. Angew Chem Int Ed. 2019;58(25):8405–9.
[28] Wang XQ, Yang SY, Tian QS, Zhong C, Qu YK, Yu YJ, et al. Multi-layer pi-stacked molecules as efficient thermally activated delayed fluorescence emitters. Angew Chem Int Ed. 2020. https://doi.org/10.1002/anie.202011384.
[29] Yang S-Y, Tian Q-S, Yu Y-J, Zou S-N, Li H-C, Khan A, et al. Sky-blue thermally activated delayed fluorescence with intramolecular spatial charge transfer based on a dibenzothiophene sulfone emitter. J Org Chem 2020;85(16):10628–37.
[30] Rajamalli P, Senthilkumar N, Gandeepan P, Huang PY, Huang MJ, Ren-Wu CZ, et al. A new molecular design based on thermally activated delayed fluorescence for highly efficient organic light emitting diodes. J Am Chem Soc 2016;138(2):628–34.
[31] Tsujimoto H, Ha DG, Markopoulos G, Chae HS, Baldo MA, Swager TM. Thermally activated delayed fluorescence and aggregation induced emission with through-space charge transfer. J Am Chem Soc 2017;139(13):4894–900.
[32] Chen XL, Jia JH, Yu R, Liao JZ, Yang MX, Lu CZ. Combining charge-transfer pathways to achieve unique thermally activated delayed fluorescence emitters for high-performance solution-processed, non-doped blue OLEDs. Angew Chem Int Ed. 2017;56(47):15006–9.
[33] Peltier JD, Heinrich B, Donnio B, Rault-Berthelot J, Jacques E, Poriel C. Electron-deficient dihydroindaceno-dithiophene regioisomers for n-type organic field-effect transistors. ACS Appl Mater Interfaces 2017;9(9):8219–32.
[34] Poriel C, Sicard L, Rault-Berthelot J. New generations of spirobifluorene regioisomers for organic electronics: tuning electronic properties with the substitution pattern. Chem Commun 2019;55(95):14238–54.
[35] Inoue S, Higashino T, Arai S, Kumai R, Matsui H, Tsuzuki S, et al. Regioisomeric control of layered crystallinity in solution-processable organic semiconductors. Chem Sci 2020;11(46):12493–505.

[36] Sicard L, Quinton C, Peltier JD, Tondelier D, Geffroy B, Biapo U, et al. Spirobifluorene regioisomerism: a structure-property relationship study. Chem Eur J 2017;23(32):7719–27.
[37] Zhang Z, Shan T, Zhang Y, Zhu L, Kong L, Liu F, et al. Isomerizing thieno[3,4-b] thiophene-based near-infrared non-fullerene acceptors towards efficient organic solar cells. J Mater Chem C 2020;8(13):4357–64.
[38] Guo J, Li X-L, Nie H, Luo W, Gan S, Hu S, et al. Achieving high-performance nondoped oleds with extremely small efficiency roll-off by combining aggregation-induced emission and thermally activated delayed fluorescence. Adv Funct Mater 2017;27(13):1606458.
[39] Ban X, Jiang W, Sun K, Lin B, Sun Y. Self-host blue dendrimer comprised of thermally activated delayed fluorescence core and bipolar dendrons for efficient solution-processable nondoped electroluminescence. ACS Appl Mater Interfaces 2017;9(8):7339–46.
[40] Ban X, Zhu A, Zhang T, Tong Z, Jiang W, Sun Y. Design of encapsulated hosts and guests for highly efficient blue and green thermally activated delayed fluorescence OLEDs based on a solution-process. Chem Commun 2017;53(86):11834–7.
[41] Liu D, Wei JY, Tian WW, Jiang W, Sun YM, Zhao Z, et al. Endowing TADF luminophors with AIE properties through adjusting flexible dendrons for highly efficient solution-processed nondoped OLEDs. Chem Sci 2020;11(27):7194–203.
[42] Huang J, Nie H, Zeng J, Zhuang Z, Gan S, Cai Y, et al. Highly Efficient nondoped OLEDs with negligible efficiency roll-off fabricated from aggregation-induced delayed fluorescence luminogens. Angew Chem Int Ed. 2017;56(42):12971–6.
[43] Guo J, Fan J, Lin L, Zeng J, Liu H, Wang C-K, et al. Mechanical insights into aggregation-induced delayed fluorescence materials with anti-kasha behavior. Adv Sci 2018;6(3):1801629.
[44] Hong Y, Lam JWY, Tang BZ. Aggregation-induced emission. Chem Soc Rev 2011; 40(11):5361–88.
[45] Lee YH, Park S, Oh J, Shin JW, Jung J, Yoo S, et al. Rigidity-induced delayed fluorescence by ortho donor-appended triarylboron compounds: record-high efficiency in pure blue fluorescent organic light-emitting diodes. ACS Appl Mater Interfaces 2017;9(28):24035–42.
[46] Liu D, Tian W, Feng Y, Zhang X, Ban X, Jiang W, et al. Achieving 20% external quantum efficiency for fully solution-processed organic light-emitting diodes based on thermally activated delayed fluorescence dendrimers with flexible chains. ACS Appl Mater Interfaces 2019;11(18):16737–48.
[47] Zhang D, Song X, Cai M, Kaji H, Duan L. Versatile indolocarbazole-isomer derivatives as highly emissive emitters and ideal hosts for thermally activated delayed fluorescent oleds with alleviated efficiency roll-off. Adv Mater 2018;30(7): 1705406.
[48] Zhang D, Zhao C, Zhang Y, Song X, Wei P, Cai M, et al. Highly efficient full-color thermally activated delayed fluorescent organic light-emitting diodes: extremely low efficiency roll-off utilizing a host with small singlet-triplet splitting. ACS Appl Mater Interfaces 2017;9(5):4769–77.
[49] Song W, Lee I, Lee JY. Host engineering for high quantum efficiency blue and white fluorescent organic light-emitting diodes. Adv Mater 2015;27(29):4358–63.